

Experiment-Based Modeling of Turbulent Flames with Inhomogeneous Inlets

Rishikesh Ranade¹ · Tarek Echekki¹ · Assaad R. Masri²

Received: 1 April 2021 / Accepted: 2 November 2021

© The Author(s), under exclusive licence to Springer Nature B.V. 2021

Abstract

An experiment-based closure framework for turbulent combustion modeling is further validated using the Sydney piloted turbulent partially premixed flames with inhomogeneous inlets. The flames are characterized by the presence of mixed mode combustion. The framework's closure is "trained" on multi-scalar measurements to construct thermo-chemical scalar statistics parameterized in terms of principal components (PCs). Three flame conditions are used for this training, while an additional flame is used for validation. The results show that the leading PCs exhibit complex features near the jet inlet where effects of partial premixing and the presence of different burning modes are strong. These features may not be captured through a strict definition for the mixture fraction or measures of reaction progress. Further downstream, the first 2 PCs tend to be reasonably correlated with parameters that are characteristic of nonpremixed flames, including the mixture fraction and the progress variable. Comparisons of the model predictions for unconditional mean and RMS for the measured quantities show a very good qualitative and quantitative agreement with experimental statistics for all 4 flames using the same closure for the PCs governing equations.

Keywords Data-based modeling \cdot Kernel density estimation \cdot Principal component analysis \cdot Artificial neural networks

1 Introduction

In two recent studies (Ranade and Echekki 2019a, b), we have introduced a novel experiment-based framework, which relies on instantaneous multi-scalar measurements to construct turbulent combustion closure models. This approach replaces the traditional physics-based moments with principal components (PCs). These PCs, which are derived from the principal component analysis (PCA) of the multi-scalar measurements,

Published online: 16 November 2021

School of Aerospace, Mechanical and Mechatronic Engineering, University of Sydney, Sydney, NSW, Australia



[☐] Tarek Echekki techekk@ncsu.edu

Department of Mechanical and Aerospace Engineering, North Carolina State University, 1840 Entrepreneur Drive, Campus Box 7910, Raleigh, NC 27695-7910, USA

represent a generic and optimum description of the composition space. The experimental data-based framework (Ranade and Echekki 2019a, b) was validated using Reynolds-averaged Navier–Stokes (RANS) simulations of the Sandia piloted jet flames, D, E and F (Barlow and Frank 1998). These validations provided an important demonstration of the framework and its model elements in well-studied flames that are subject to extinction and reignition.

The Sydney piloted jet diffusion flames with inhomogeneous inlets (Meares and Masri 2014; Barlow et al. 2015; Meares et al. 2015; Cutcher et al. 2017) provide a natural extension to the Sandia flames. These flames, like the Sandia flames, exhibit non-equilibrium effects. They also feature a range of mixture inhomogeneities at the burner inlet. These inhomogeneities result in varying degrees of partial premixing and the presence of multiple modes of combustion. Several studies based on variations of different closure models have been carried out to accurately model the Sydney flames with inhomogeneous inlets (Wu and Ihme 2016; Maio et al. 2021; Perry et al. 2017; Galindo et al. 2017; Kleinheinz et al. 2017; Ji et al. 2018; Galindo-Lopez et al. 2018; Kim and Kim 2017; Perry and Mueller 2019). They have sought to address the presence of different modes of combustion through different strategies, including a multi-regime combustion model (Kleinheinz et al. 2017), which is built on the flamelet approach, a two-mixture fraction flamelet model (Perry et al. 2017), the implementation of the multi-environment PDF approach with tabulated chemistry based on premixed and nonpremixed flames solutions (Galindo-Lopez et al. 2018) and the multiple mapping conditioning (MMC) approach (Galindo et al. 2017; Galindo-Lopez et al. 2018).

In this work, the experiment-based framework is used to model four Sydney piloted jet flames at different mixture and velocity inlet conditions (Meares and Masri 2014; Barlow et al. 2015; Meares et al. 2015; Cutcher et al. 2017). These flames exhibit variations in fuel inlet velocities and mixture conditions resulting in various degrees of extinction and reignition as well as variations in the in the dominant combustion mode at different downstream distances. Out of the 4 flames, the data used to determine the PCs and associated statistics is based only on 3 of these flames. Therefore, a principal objective of this study is to investigate whether data based on a set of flames can be used to model a similar set of flames. Within this objective, it is important to investigate whether a relatively low number of PCs can still represent the additional complexity of multi-mode combustion, especially in the near field of these flames.

In Sect. 2, we briefly present the formulation of the closure framework and information related to different preprocessing steps. This is followed, in Sect. 3, by a discussion of PCs generated from the experimental data relative to the Sandia flames and downstream conditions and the a priori and a posteriori validation of the framework. Finally, conclusions and a discussion of future work are presented in Sect. 4.

2 Model Formulation

The model formulation is briefly stated here since it follows the same procedure adopted in Ranade and Echekki 2019b. The transported PCs are derived using a linear transformation from a normalized set of representative thermo-chemical scalars, which in the present study correspond to the measured quantities (temperature and major species). The governing equations for the low Mach number formulation are:



Momentum:
$$\frac{\partial \overline{\rho} \widetilde{u}_i}{\partial t} + \frac{\partial \overline{\rho} \widetilde{u}_i \widetilde{u}_j}{\partial x_i} = -\frac{\partial \overline{\rho}}{\partial x_i} + \frac{\partial}{\partial x_i} \left[2\overline{\rho} (v_T + v) \widetilde{S}_{ij} \right], i = 1, 2, 3.$$
 (1)

PCs:
$$\frac{\partial \overline{\rho} \tilde{\phi}_{k}}{\partial t} + \frac{\partial \overline{\rho} \tilde{u}_{j} \tilde{\phi}_{k}}{\partial x_{j}} = \frac{\partial}{\partial x_{j}} \left[\overline{\rho} \left(\frac{v_{T}}{Sc_{T}} + D_{k} \right) \frac{\partial \tilde{\phi}_{k}}{\partial x_{j}} \right] + \overline{s}_{\phi_{k}}, k = 1, \dots, N_{PC}$$
 (2)

In the above expressions, the symbols "—" and "—" correspond to Reynolds and Favre averaging, respectively. \tilde{u}_i and $\tilde{\phi}_k$ represent the *i*th direction velocity component and the *k*th PC, respectively. v_T is and Sc_T are the turbulent kinematic viscosity and Schmidt number and S_{ij} is the ij component of the rate-of-strain tensor. In addition to v_T , the mean PC source terms, \bar{s}_{ϕ_k} , and the averaged density $\bar{\rho}$ are the main closure terms in Eqs. (1) and (2); and both \bar{s}_{ϕ_k} and $\bar{\rho}$ are obtained from the data-based framework.

The unconditional means of the density and the PC source terms are evaluated using a convolution of their conditional means with the PCs' joint PDFs:

$$\bar{\rho} = \int \langle \rho | \mathbf{\phi} \rangle P(\mathbf{\phi}; \tilde{\mathbf{\phi}}) d\mathbf{\phi} \text{ and } \bar{s}_{\mathbf{\phi}_{k}}(\mathbf{\phi}) = \int \langle s_{\mathbf{\phi}_{k}} | \mathbf{\phi} \rangle P(\mathbf{\phi}; \tilde{\mathbf{\phi}}) d\mathbf{\phi}$$
(3)

where $\langle \rho | \phi \rangle$, $\langle \theta_k | \phi \rangle$ and $\langle s_{\phi_k} | \phi \rangle$ represent the means of density, thermo-chemical scalars, and PC source terms, respectively, conditioned on the PCs. $P(\phi; \tilde{\phi})$ is the joint PCs PDF. Therefore, these conditional means and PDFs are the quantities that are extracted directly from the experimental data. Although not needed for the solution of Eqs. (1) and (2), the thermo-chemical scalars (temperature and measured species) unconditional means can be evaluated as well using:

$$\tilde{\theta}_{k}(\tilde{\mathbf{\Phi}}) = \frac{\int \rho |\mathbf{\Phi}\theta_{k}| \mathbf{\Phi} P(\mathbf{\Phi}; \tilde{\mathbf{\Phi}}) d\mathbf{\Phi}}{\bar{\rho}} \tag{4}$$

As outlined in Ref. (Ranade and Echekki 2019b), the procedure for evaluating \bar{s}_{ϕ_k} and $\bar{\rho}$ and $P(\phi; \tilde{\phi})$ is as follows:

First, the measured thermo-chemical scalars are normalized to vary from − 1 to 1. PCs are determined from an eigen-decomposition of the normalized data's covariance matrix. The PCs are ordered by the magnitude of their corresponding eigenvalues. The number of retained PCs, N_{PC}, is determined based on a threshold on the cumulative variance contributed by the leading PCs. Here we adopt a threshold of 99%. The resulting PCs are related to the original thermo-chemical scalars (Mirgolbabaei and Echekki 2014):

$$\mathbf{\phi} = \mathbf{A}^{\mathrm{T}}\mathbf{\theta},\tag{5}$$

where the constant matrix A^T contains the retained N_{PC} PCs eigenvectors. Following PCA, the conditional means are computed for the measured thermo-chemical scalars and density using a binning procedure. A similar relation expresses the PCs' chemical sources in terms of thermo-chemical scalars' sources:

$$\mathbf{s}_{\mathbf{\phi}} = \mathbf{A}^{\mathrm{T}} \mathbf{s}_{\mathbf{\theta}}.\tag{6}$$

however the evaluation of s_{ϕ} within a prescribed chemical mechanism also requires the evaluation of the concentration of additional species that are not measured. Relying on



the raw measured data to recover these species invariably results in greater uncertainty in the evaluation of s_{ϕ} .

- 2. The missing species are recovered by first clustering the data based on the values of the PCs using self-organizing maps (SOMs) (Kohonen 1982), then, carrying out pairwise mixing stirred reactor (PMSR) simulations (Pope 1997; Yang and Pope 1998) in each cluster. The initial states of the particles within the PMSR correspond to the experimental measurements, while the missing species are set to 0. Following the PMSR calculations, conditional means for the species (measured and recovered) updated solutions from PMSR and the PCs chemical source terms (Eq. (6)) are determined. These means are implemented using a 2D binning procedure for the 2-PC parameterization of the composition space.
- 3. The PCs joint PDFs are constructed at each measurement position using the multidimensional kernel density estimation (KDE) technique (Bowman and Azzalini 1997). KDE accommodates different shapes in the statistical distribution and can be implemented without assuming statistical dependence between the PCs. A *d*-dimensional KDE is expressed as a sum of kernel functions centered on model-determined points from the sample data (Bowman and Azzalini 1997) at any given measurement position:

$$P(\mathbf{\phi}; \tilde{\mathbf{\phi}}) = \frac{1}{nh} \sum_{i=1}^{n} K\left(\frac{\mathbf{\phi} - \hat{\mathbf{\phi}}_{i}}{h}\right)$$
 (7)

where K is the kernel function, h is the bandwidth and $\hat{\phi}_i$ are the n samples of the selected PCs for a given measurement position, which is also characterized by the unconditional means of the PCs, $\tilde{\phi}$. ϕ corresponds to the instantaneous PCs at a given position in space. In the present study, the KDE-constructed joint PCs' PDF is used explicitly to determine the unconditional reaction rate mean (Eq. (3)). The kernel function adopted is the Gaussian function.

With the available data and the PMSR calculations, the PCs unconditional means can be evaluated using Eq. (3). Finally, artificial neural networks (ANN) are used to construct regressions for the unconditional means as functions of the Favre averaged PCs. As a multi-variate, non-linear regression method, ANN has found use in different applications in combustion (Christo et al. 1995, 1996a, b; Blasco et al. 1998, 1999, 2000; Chen et al. 2000; Ihme et al. 2008, 2009; Sen and Menon 2010; Sen et al. 2010; Chatzopoulos and Rigopoulos 2013; Ranade et al. 2019a, b, 2021; Franke et al. 2017; Owoyele et al. 2019). In the present study, separate networks are constructed for different output variables in terms of the retained PCs unconditional means. The PC source terms networks consist of input and output layers and 3 hidden layers; and the number of neurons in each hidden layer is 30, 22 and 15, respectively. The thermo-chemical scalar networks are simpler and contain 2 hidden layers with 30 and 15 neurons, respectively. The data set is divided into training, validation and testing set in the following ratio, 70/15/15. The ANN training is implemented until the mean squared error between the network output and target value for the testing data is below 10^{-6} . The entire training process takes approximately an hour on a single processor of an Intel Xeon CPU.

As a data-based modeling framework, our approach benefits from an a priori validation step to determine the adequacy of the closure approach on the data used for training the model, including the adequacy of the retained PCs. The training relies primarily on characterizing the data in composition space. The ability of the governing Eqs. (1) and (2) to predict thermo-chemical scalars statistics also depends largely on the closure for



the PCs source terms. Despite the potential role of experimental uncertainty in determining the species reaction rates in PMSR, pairwise mixing in this reactor combined with reaction significantly reduces this contribution from experimental uncertainty as demonstrated in the a posteriori results. In contrast, statistics associated with conditional means and joint PCs PDFs tend to be inherently less sensitive to this uncertainty.

3 Results and discussion

In this section, we present results of our closure methodology implemented on four Sydney piloted jet flames with inhomogeneous inlets (Meares and Masri 2014; Barlow et al. 2015; Meares et al. 2015; Cutcher et al. 2017).

3.1 Flame Description

The modified Sydney piloted jet burner was developed by Meares et al. (2014) to study turbulent flame characteristics under the presence of inhomogeneous inlet conditions. The burner consists of an inner tube and an outer concentric tube with diameters of 4 and 7.5 mm, respectively. In the FJ flame configurations considered, the fuel is injected through the inner tube while co-flow air is injected through the outer tube. The outer tube is surrounded by a pilot stream, which has a diameter of 18 mm. The fuel jet comprises of methane (CP grade) with 99% CH₄ at a temperature of 294 K. The 5-gas (5GP) pilot stream in each case is a mixture of C_2H_2 , H_2 , CO_2 , N_2 and air with an adiabatic flame temperature of 2226 K and a bulk inlet velocity of 3.7 m/s. The co-flow consists of air at 291 K and an inlet velocity of 15 m/s. The inner tube is recessed and can slide within the outer tube to allow for various degrees of partial premixing for a recess distance, L_r , of up to 500 mm from the exit plane. A fully recessed inner tube allows effective premixing of fuel and air and corresponds to a homogeneous inlet condition. In contrast, when $L_r = 0$, such a condition corresponds to a fully inhomogeneous inlet condition.

In the present study, the experiment-based framework is validated for 4 different flame conditions. They represent two recess lengths of 75 mm and 300 mm (Lr75 and Lr300) and different fuel inlet speeds, U_j , which correspond to 57, 59, 80 and 103 m/s. These flames are summarized in Table 1.

As the table indicates, the data from 3 of the flames are used for model training to determine the closure for the unconditional means for the density and the PCs source terms. They include FJ200-5GP-Lr75-57, FJ200-5GP-Lr75-80 and FJ200-5GP-Lr300-59 (Meares and Masri 2014; Barlow et al. 2015; Meares et al. 2015; Cutcher et al. 2017), for which velocity inlet data is also available, while FJ200-5GP-Lr75-103

Table 1 Characteristics of the studied Sydney flames

Flame	L_r (mm)	U_j (m/s)	Validation (V)/Training (T)
FJ200-5GP-Lr075-57	75	57	V & T
FJ200-5GP-Lr075-80	75	80	V & T
FJ200-5GP-Lr075-103	75	103	V
FJ200-5GP-Lr300-59	300	59	V & T



is modeled with this 3-flame data. This latter flame has a higher fuel jet inlet velocity than the corresponding 57 and 80 m/s inlet velocities, resulting in higher occurrences of extinction conditions. FJ200-5GP-Lr75-57, FJ200-5GP-Lr75-80, FJ200-5GP-Lr300-59 and FJ200-5GP-Lr75-103 are at 50%, 70%, 70% and 80% from experimentally measured blow-off velocity, respectively.

The 75 mm recess length corresponds to highly inhomogeneous conditions; while the 300 mm recess length results in a near-homogeneous condition at the burner inlet. Although measurements are available corresponding to different mixture conditions at the burner inlet, we have chosen 3 flames for training the data primarily because of the availability of inlet velocity measurements, as suggested above. It is likely that a different combination of flames used for training would yield slightly different abilities to predict all flames. In the present study, we have not investigated such combinations. However, the framework relies on the presence of variability in the data, which is manifested in the presence of different inlet conditions, the representation of different combustion modes and conditions for extinction and reignition. The experimental data corresponding to the 4 flames consist of instantaneous measurements collected at different downstream of x/d=1, 2, 3, 5, 7, 10, 12, 15, 20 and 30 where x is the downstream distance and d is the fuel jet diameter and radial positions. Each measurement position includes from 2000 to 3000 single shot multi-scalar measurements. The experimental data includes line measurements of temperature in addition the following species: H₂O, CO_2 , O_2 , CH_4 , CO and H_2 .

In contrast with the Sandia piloted flames that we have investigated recently (Ranade and Echekki 2019a, b), the present Sydney flames data feature additional complexities. The first, as outlined earlier, is associated with the presence of multiple modes of combustion associated with mixture inlet inhomogeneity in the Sydney flames. From the measurement adequacy standpoint, the Sydney flames data does not include OH. In the Sandia flames studies (Ranade and Echekki 2019a, b), OH is the major contributor to the third PC. As a radical species, its presence is an important indicator of the presence of reaction. A consequence of not including OH, implementing the threshold of 99% for the selection of the PCs results in the selection of 2 PCs compared to 3 PCs in the Sandia flames (Ranade and Echekki 2019a, b). This, of course, does not suggest that less PCs are needed to model the Sydney flames for comparable abilities to predict statistics. Therefore, it remains to be determined whether not measuring OH will significantly impact the predictions of the remaining scalar statistics as well as the closure for the PCs source terms.

3.2 A Priori Results

Before implementing the experimental data-based framework to develop closure models for a CFD simulation, we would like to evaluate the adequacy of the different elements of the framework with respect to the experimental data of Sydney flames. In the a priori studies, we validate the robustness of the closure framework by reconstructing Favre averages of measured thermo-chemical scalars using Eq. (4) and comparing them with experimentally measured averages, which are readily available from the multiple shot measurements. These results will allow us to evaluate the number of PCs required for an accurate representation of the composition space and to determine the adequacy of conditional means and joint PDFs amidst experimental uncertainty.



3.2.1 PCA Parameterization

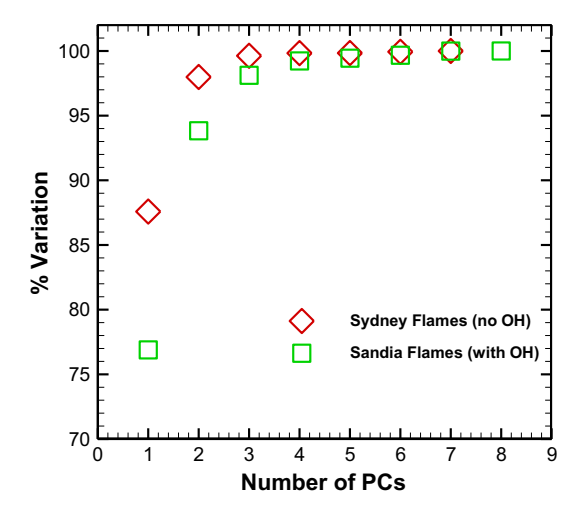
Figure 1 shows a comparison of the scree plots for the Sydney flames based on the 3 flame conditions used for the training the framework and the Sandia flames based on flames D, E and F (Barlow and Frank 1998). These plots show the percent cumulative variance captured by the PCs. The contribution of each PC to the total variance of the data is expressed as the ratio of the eigenvalue associated with that PC and the sum of all the PCs eigenvalues. A principal advantage of PCA in combustion problems is that the bulk of the data variance is represented by the first few PCs, thus justifying the assumption of the presence of low-dimensional manifolds in composition space. Assessing the cumulative contribution of these first PCs to the entire data can help identify the number of PCs that can adequately represent the composition space accessed by experimental data. The a priori assessment presented in Sec. 3.2.2 provides an additional validation for the adequacy of this contribution. As argued above, 2 PCs without OH in the case of the Sydney flames capture approximately as much variation as 3 PCs with OH in the Sandia flames. In a previous study (Ranade and Echekki 2019a, b), we have observed that OH played an important role in the makeup of the third and fourth PCs in the Sandia flames.

To further understand the contribution of the measured thermo-chemical scalars to the PCs, we re-write Eq. (5) in terms of the contributing thermo-chemical scalars in the Sydney flames as follows:

$$\begin{pmatrix} \phi_1 \\ \phi_2 \\ \phi_3 \\ \phi_4 \\ \phi_5 \\ \phi_6 \\ \phi_7 \end{pmatrix} = \begin{pmatrix} \mathbf{0.612} & -\mathbf{0.618} & -0.085 & 0.184 & 0.304 & 0.012 & 0.331 \\ -0.297 & -\mathbf{0.414} & \mathbf{0.832} & -0.065 & -0.139 & 0.008 & 0.154 \\ -0.295 & 0.126 & -0.240 & 0.020 & -0.202 & 0.040 & \mathbf{0.893} \\ -\mathbf{0.659} & -\mathbf{0.455} & -0.359 & -0.009 & \mathbf{0.460} & 0.006 & -0.145 \\ 0.028 & \mathbf{0.448} & 0.315 & -0.140 & \mathbf{0.795} & -0.044 & 0.216 \\ 0.130 & -0.149 & -0.120 & -\mathbf{0.966} & -0.059 & -0.083 & 0.044 \\ 0.023 & 0.016 & 0.010 & -0.090 & 0.033 & \mathbf{0.995} & -0.027 \end{pmatrix} \begin{pmatrix} T^* \\ Y^*_{0_0} \\ Y^*_{CL_4} \\ Y^*_{H_1O} \\ Y^*_{CO} \\ Y^*_{CO} \end{pmatrix}$$

Note that the superscript "*" indicates a normalization of the thermo-chemical scalars using minimum and maximum values in the data such that their values range from -1 to

Fig. 1 Scree plot comparison based on instantaneous data of Sydney flames (FI200-5GP-Lr75-80 and FI200-5GP-Lr300-59) (Meares and Masri 2014; Barlow et al. 2015; Meares et al. 2015; Cutcher et al. 2017) and Sandia Flames (D, E and F) (Barlow and Frank 1998)





1. The normalization accommodates the different magnitudes of the measured quantities. As implemented in Ref. (Ranade and Echekki 2019a), we are highlighting values of the coefficients in the ${\bf A}^{\rm T}$ matrix with magnitudes greater than 0.4. This choice is arbitrary, and it attempts to highlight the major contributing thermo-chemical scalars to the PCs. Also, for comparison, we reproduce the same relations for the Sandia piloted flames with and without OH in Eqs. (9) and (10), respectively. In Eq. (9), we place the normalized OH mass fraction at the bottom of the thermo-chemical scalars' vector and place PC₄, which is dominated by the OH, at the bottom of the PC vector.

$$\begin{pmatrix} \phi_1 \\ \phi_2 \\ \phi_3 \\ \phi_5 \\ \phi_6 \\ \phi_7 \\ \phi_8 \\ \phi_4 \end{pmatrix} = \begin{pmatrix} \boxed{0.514} & -0.508 & -0.127 & 0.428 & 0.429 & 0.172 & \boxed{0.098} & 0.237 \\ -0.042 & -0.219 & 0.899 & 0.026 & -0.088 & 0.277 & 0.226 & -0.077 \\ 0.074 & 0.019 & 0.374 & -0.100 & 0.226 & -0.595 & -0.464 & -0.473 \\ 0.159 & 0.034 & 0.025 & -0.120 & -0.028 & 0.584 & -0.781 & -0.089 \\ -0.325 & -0.080 & -0.043 & -0.555 & 0.722 & 0.197 & 0.135 & 0.006 \\ 0.665 & -0.016 & -0.020 & -0.663 & -0.249 & -0.021 & 0.220 & 0.082 \\ 0.259 & -0.062 & 0.098 & 0.021 & 0.264 & -0.366 & -0.139 & -0.834 \end{pmatrix} \begin{pmatrix} T^* \\ Y^*_{0_0} \\ Y^*_{CL_4} \\ Y^*_{H_2O} \\ Y^*_{CO_2} \\ Y^*_{H_2} \\ Y^*_{CO} \\ Y^*_{OH} \end{pmatrix}$$

$$\begin{pmatrix} \phi_1 \\ \phi_2 \\ \phi_3 \\ \phi_4 \\ \phi_5 \\ \phi_6 \\ \phi_7 \end{pmatrix} = \begin{pmatrix} \textbf{0.513} & -\textbf{0.510} & -0.181 & \textbf{0.434} & \textbf{0.447} & 0.126 & 0.227 \\ -0.044 & -0.205 & \textbf{0.878} & 0.025 & -0.092 & 0.265 & 0.324 \\ -0.197 & 0.088 & -\textbf{0.414} & 0.023 & -0.339 & \textbf{0.498} & \textbf{0.647} \\ -0.158 & -0.148 & -0.010 & 0.009 & -0.058 & -\textbf{0.802} & \textbf{0.553} \\ \textbf{0.566} & 0.199 & 0.069 & 0.385 & -\textbf{0.679} & -0.145 & -0.072 \\ -\textbf{0.590} & -0.361 & -0.045 & \textbf{0.619} & -0.220 & 0.001 & -0.298 \\ -0.121 & \textbf{0.706} & 0.133 & \textbf{0.528} & \textbf{0.405} & -0.020 & 0.161 \end{pmatrix} \begin{pmatrix} T^* \\ Y_{\odot} \\ Y_{\odot}^* \\ Y_{CO} \\ Y_{\odot}^* \\ Y_{\odot}^* \\ Y_{\odot}^* \end{pmatrix}$$

For the Sandia flames, we have identified the contributions of PC_1 and PC_2 , as being strongly correlated with the reaction progress variable (i.e., heavily weighted by the reactants, products, or temperature) and the mixture fraction (i.e., heavily weighted by C/H containing species vs. O containing species and varies monotonically with the mixture fraction). We see that by omitting OH, the first two PCs still represent a progress variable and a mixture fraction. The most important variations arise at the remaining PCs as indicated in Eq. (9).

Similar contributions are found for the Sydney flames based on the coefficients of the matrix of eigenvectors corresponding to the first 2 PCs (i.e., the first 2 rows of these matrices); even though the magnitudes of these coefficients are different. The most important differences between the Sandia flames and the Sydney flames for the first PC are related to the contributions of the products H_2O and CO_2 and the intermediate H_2 . Part of these differences can be attributed to the ranges of values used in the normalization, which, for the Sydney flames, correspond to the different modes of combustion present in these flames. These differences will be considered below. For the second PC, the dominant contribution in the Sandia flames is from the fuel. However, in the Sydney flames, the oxidizer is also important.

Equations (11–13) re-write Eq. (5) for the Sydney flames for 3 different ranges of x/d. The first range shown in Eq. (11) corresponds to a PCA that includes data from x/d=1 to 7 near the jet inlet where the mixtures burn in mixed modes (premixed and nonpremixed). The second range presented in Eq. (12) corresponds to data from x/d=7 to 10, which



represents more-or-less the transition region prior to non-premixed combustion. Finally, the last range shown in Eq. (13) corresponds to data at x/d=12 and above. However, it is important to note that the modeling framework is based on the cumulative data from all downstream distances and all flames considered for training as presented in Eq. (7).

$$1 \leq \frac{x}{d} \leq 7: \begin{pmatrix} \phi_1 \\ \phi_2 \\ \phi_3 \\ \phi_4 \\ \phi_5 \\ \phi_6 \\ \phi_7 \end{pmatrix} = \begin{pmatrix} \mathbf{0.649} & -0.558 & -0.171 & 0.182 & 0.342 & 0.022 & 0.295 \\ -0.152 & -0.483 & \mathbf{0.858} & -0.042 & -0.066 & 0.001 & 0.018 \\ -0.272 & 0.065 & -0.047 & -0.001 & -0.208 & 0.087 & \mathbf{0.932} \\ -0.677 & -0.410 & -0.309 & -0.006 & \mathbf{0.522} & -0.021 & -0.067 \\ \mathbf{0.677} & \mathbf{0.522} & 0.360 & -0.007 & \mathbf{0.742} & -0.094 & 0.179 \\ 0.125 & -0.094 & -0.076 & -\mathbf{0.944} & 0.031 & -0.268 & 0.070 \\ 0.037 & 0.023 & 0.014 & -0.270 & 0.104 & \mathbf{0.994} & -0.056 \end{pmatrix} \begin{pmatrix} T_* \\ Y_{0_2} \\ Y_{CO} \\ Y_{H_2}^* \\ Y_{CO} \\ Y_{CO}^* \\ Y_{$$

From the different data ranges, there is significant similarity between the dominant terms, which contribute to the first two PCs, as well as there are similarities between the eigenvector matrices and those of the combined data for the Sydney flames (see Eq. (8)). Again, the magnitudes of the coefficients can be attributed to the differences in the ranges of values of the thermo-chemical scalars due to different modes of combustion at the different downstream distances. However, the most important change as a function of downstream distance is observed for the second PC where the main contribution is shifted to the fuel at the expense of the oxidizer as the dominant combustion mode shifts to nonpremixed burning. This shift is present in the contribution to the PCs of the Sandia flames. Beyond the second PC, the relative magnitudes of the coefficients exhibit similar trends to the combined data for the Sydney flames.

It is important to note that in all the above comparisons, the first 2 PCs account for approximately 99% of the data variance. Therefore, we expect these 2 PCs to provide an adequate representation of the transitions in combustion modes in the Sydney flames. Adding the third PC can potentially improve the prediction of CO given the important contribution of this species for this PC. However, this addition may come at the expense of model complexity. This complexity translates into a higher dimension for the conditional means and the joint PCs PDFs. Again, much of the difference between the Sandia



and the Sydney flames appears in the contributions to the second PC. It goes without saying that the degrees of partial premixing occurring near the burner inlet clouds the definitions of a reference state for pure fuel and oxidizer (Barlow et al. 2015). Here, we speculate that the preservation of the importance of both the fuel and oxidizer near the inlet indicates the importance of lean and rich premixed burning at these conditions.

Barlow et al. (2017) have investigated 3 different definitions of progress variable in the Sydney flames, 2 based on weighted sums of the products and one based on the oxygen mass fractions in the products. Although the progress variable based on oxygen is identified as a good choice for post-processing results from experimental measurements, the progress variables do not exhibit statistical independence with the mixture fraction, raising important challenges for traditional modeling strategies. Regardless, it is clear that a choice of parameters to characterize the Sydney flames is not trivial; yet PCA is able to extract such parameters as a linear combination of the representative scalars for the data.

The above observations suggest that adopting a traditional non-premixed flamelet/progress variable (FPV) approach may not be adequate to accommodate the different regimes encountered in the Sydney flames as a function of downstream distance and recess length. Nonetheless, variants of this approach have been applied to the Sydney flames.

Perry et al. (2017) proposed a two-mixture fraction model to accommodate the fuel-stream variations at the inlet. Their study investigated 2 flame conditions, FJ200-5GP-Lr300-59 and FJ200-5GP-Lr75-57. Kleinheinz et al. (2017) applied a multi-regime flame-let model to accommodate variations in the combustion mode as a function of downstream distance. Their study covered 4 different flame configurations, FJ200-5GP-Lr000-57, FJ200-5GP-Lr75-80, FJ200-5GP-Lr300-59 and FJ200-3GP-Lr100-82. Kim and Kim (2017) used the flamelet generated manifolds (FGM) approach combined with the multi-environment PDF approach to study the Sydney flames and premixed and non-premixed flamelet libraries. Their study included the near-homogeneous and inhomogeneous flames, FJ200-5GP-Lr300-59 and FJ200-Lr75-57. These studies provided adequate comparisons between flamelet-based models and experiment, although comparisons were made for only a subset of the measured scalars.

Having discussed the contributions of various thermo-chemical scalars to the PCs at different downstream distances, our subsequent discussion will be based on PCs that are constructed based on 3 flames and all downstream distances combined. This includes our a posteriori analysis where the governing Eqs. (1) and (2) are solved using only one pair of PCs based on the transformation presented in Eq. (8). Figure 2 shows scatter plots of the first 2 PCs vs. the Bilger's mixture fraction (Barlow et al. 2017) for flames FJ200-5GP-Lr75-57 (the "inhomogeneous inlet" case) and FJ200-5GP-Lr300-59 (the "near-homogeneous inlet" case) at a downstream distance of one jet diameter (x/d=1). The scatter points are color-coded based on temperature (red symbols for temperatures above 1000 K and black symbols for temperatures below 1000 K). The red vertical dashed lines mark the stoichiometric mixture fraction. With one key difference, the first PC's profiles are similar to the temperature profiles discussed by Barlow et al. (Barlow et al. 2015). This difference is exhibited by the trailing cold mixing contributions from the fuel as shown by the nearly linear scatter profiles from the stoichiometric mixture fraction to higher values. The scatter around the stoichiometric mixture fraction exhibits the near-vertical trajectories for PC₁ for the inhomogeneous inlet case indicating a wide range of burning and non-burning conditions and the conditions at the pilot (Barlow et al. 2015).

In contrast, PC₂ for the inhomogeneous case is reasonably correlated with the mixture fraction and reproduces the trends observed in the Sandia flames. In the near-homogeneous



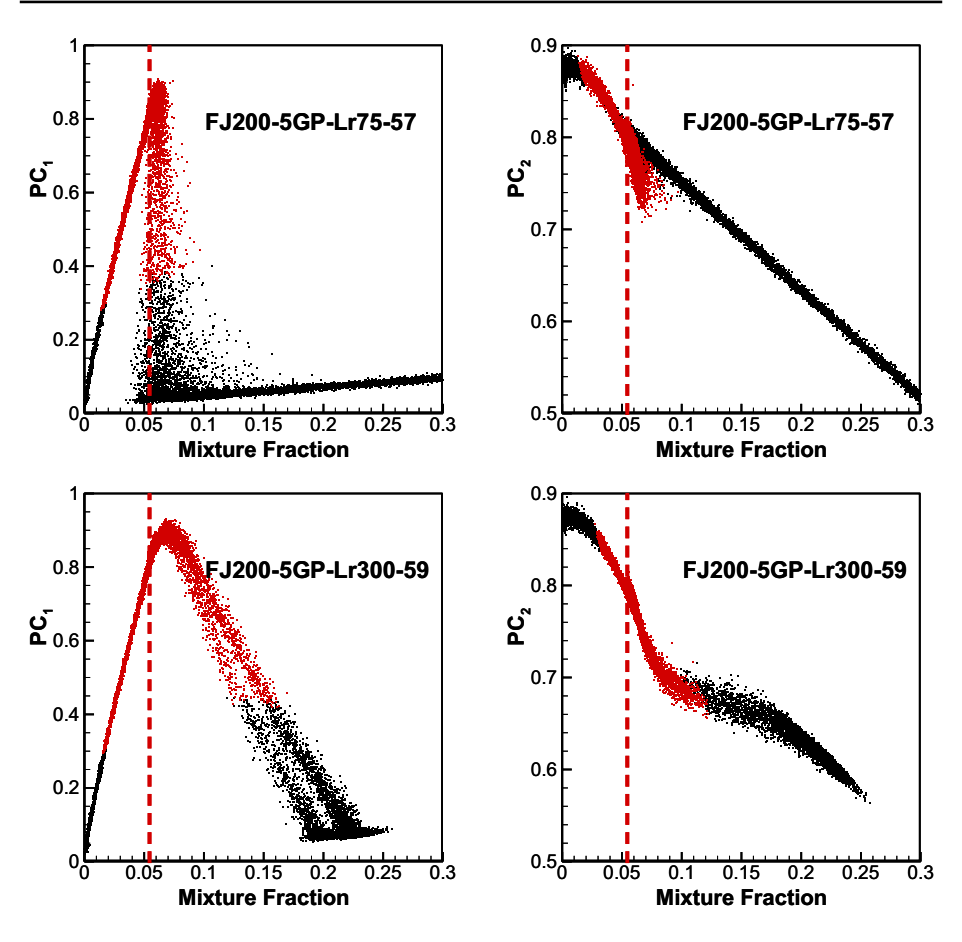


Fig. 2 Scatter plots of PC₁ and PC₂ versus the Bilger mixture fraction for flames FJ200-5GP-Lr75-57 and FJ200-5GP-Lr300-59 at x/d=1. Red scatter points: $T \ge 1000$ K; black scatter points: T < 1000 K.

flame, FJ200-5GP-Lr300-59, PC₂ is monotonic with the mixture fraction and exhibits a dip in its profiles at slightly rich conditions.

Figure 3 shows the same scatter plots shown in Fig. 2 for the case of x/d = 10. The figure shows that the qualitative trends for the inhomogeneous and near-homogeneous flames are similar further downstream of the jet inlet as the mixture transitions to a primarily nonpremixed combustion mode. These are the same trends observed for other thermo-chemical scalars (T and CH₄, O₂ and CO mass fractions) in Ref. (Barlow et al. 2015). As expected, the differences in statistics between the two flames are primarily attributed to the nature of reaction at the inlet due to partial premixing.

3.2.2 A Priori Radial Plot Comparisons

The present modeling framework includes measures of quality control that can be established through a priori comparisons of the measured scalars' statistics obtained directly from experimental measurements or from the convolution of the scalars' conditional means with the PCs joint PDFs. These comparisons provide a crucial assessment of the adequacy



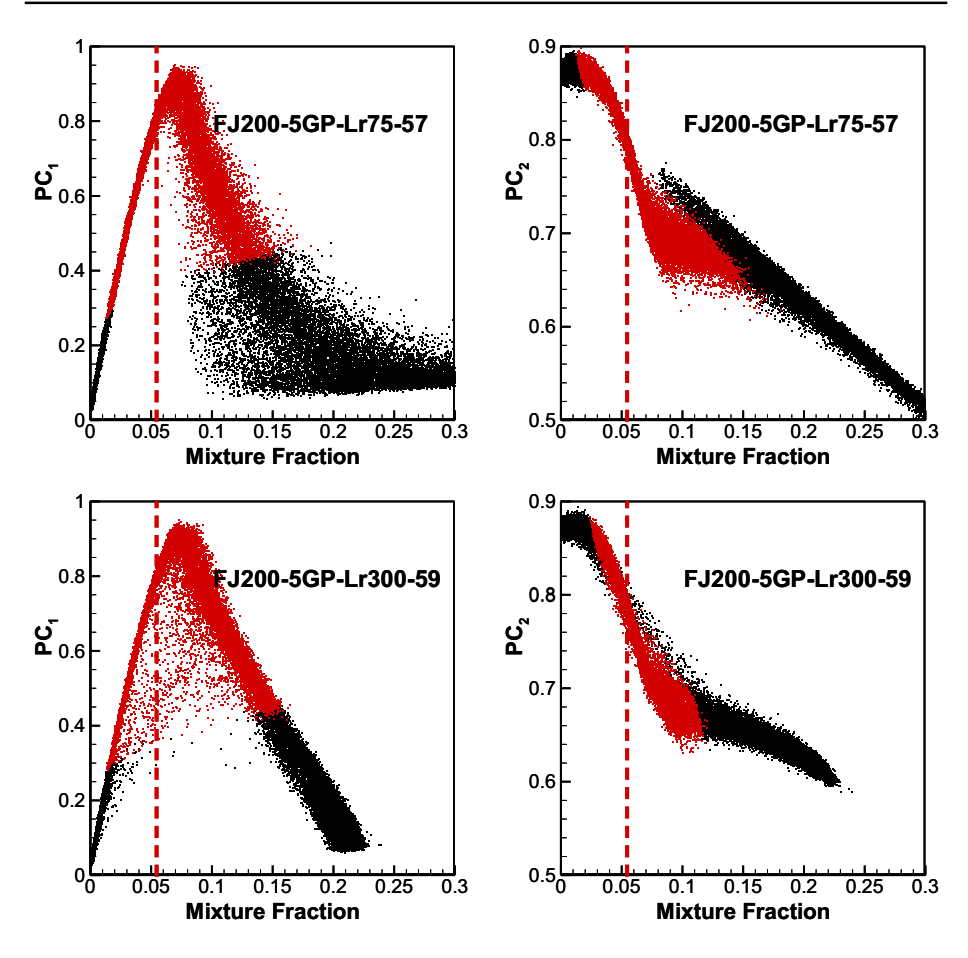


Fig. 3 Scatter plots of PC_1 and PC_2 vs. the Bilger mixture fraction for flames FJ200-5GP-Lr75-57 and FJ200-5GP-Lr300-59 at x/d = 10

of the number of PCs retained as well as the models for the scalars' conditional means and the PCs joint PDFs.

Figure 4 shows such comparisons based on 2 PCs for radial profiles of the unconditional Favre-averaged means of temperature and H_2 , CO and H_2 O mass fractions at five different axial locations, x/d=1, 5, 10, 15, 20 and 30 and for Sydney flame FJ200-5GP-Lr75-57. Similar comparisons are obtained for the other 2 flames considered for training the modeling framework. The conditional means are constructed from a compilation of all the instantaneous measurements of the 3 flames, while the joint PDFs are constructed at the different measurement positions.

The figure shows that the radial profiles of T, H_2 , CO and H_2O , obtained using Eq. (4) are in excellent agreement with the experimental means. Although not shown here, other measured scalars such as O_2 , CH_4 and CO_2 show a similar agreement. Such agreements are necessary, yet insufficient, conditions for the success of the modeling framework. The most important ingredient for this success is the ability to model the closure terms in the PCs governing equations: models: \bar{s}_{ϕ_k} and $\bar{\rho}$, which are strongly coupled with other transport



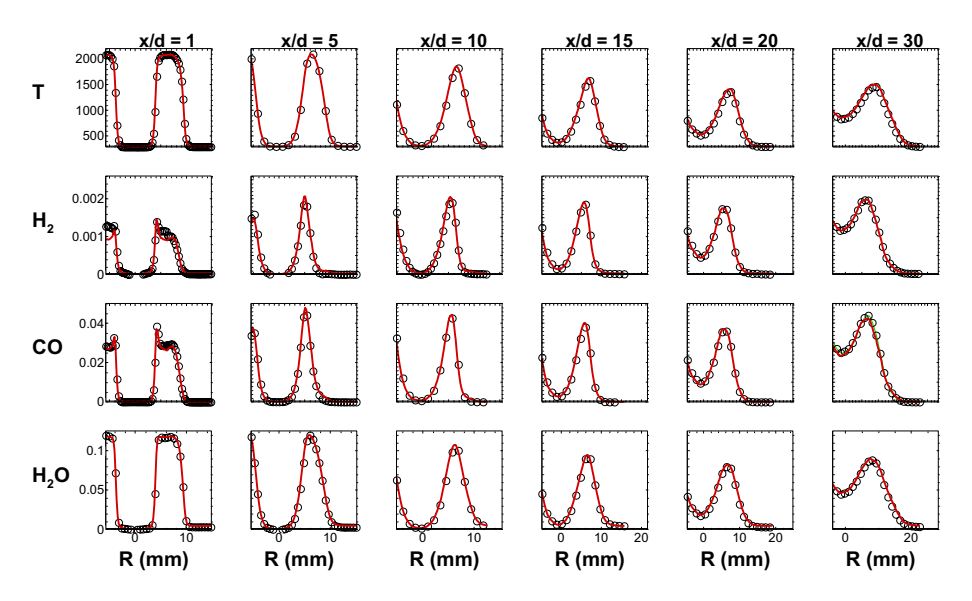


Fig. 4 A priori radial plot comparison of closure framework (line) and experimental data (symbol) for Sydney flame FJ200-5GP-Lr75-57

terms in the PCs' governing equations. Based on the above results, our model implementation is based on the transport of 2 PCs, which are obtained using PCA on the 3 flame selected flames and at all downstream distances where data is available.

3.3 A Posteriori Results

For the a posteriori studies, the PC transport equations are solved using RANS for the 4 flames considered, while the data used for the construction of the framework is based on 3 of these flames.

3.3.1 RANS setup

The RANS simulations are carried out in Ansys Fluent 17.0 with the governing Eqs. (1) and (2) are solved in their conservative forms. A realizable k- ε model it used to model the turbulent viscosity (Shih et al. 1995) thus also requiring the solutions for the turbulent kinetic energy, q, and its dissipation rate, ε . The simulation is set-up on a 2-D axis-symmetric domain and a structured, quadrilateral mesh with a cell count of close to 100,000 cells. A highly refined mesh is considered to ensure grid independence.

The closure model is integrated into the solver using user-defined functions (UDF) and the PC transport equations are defined as user-defined scalars (UDS). The Poisson equation for the dynamic pressure is solved to enforce continuity. First-order upwind schemes are used for q, ϵ and the PCs transport equations, while the pressure and momentum equations are resolved to second order accuracy. The solution convergence is tracked by monitoring the residuals of all transported quantities. The solution converges when the relative residual falls below 10^{-5} . Since this is a steady-state run, an initial flame solution is provided. This solution is obtained by interpolating the radial profiles from experiments at



different downstream distances. The inlet conditions for the velocity, the turbulence parameters and the PCs are prescribed with values provided with the experimental database for flames FJ200-5GP-Lr75-57, FJ200-5GP-Lr75-80 and FJ200-5GP-Lr300-59. Since the inlet velocity information is not available for flame FJ200-5GP-Lr75-103, we extrapolate the inlet information for the velocity field from the provided profiles for FJ200-5GP-Lr75-57 and FJ200-5GP-Lr75-80. A turbulent Schmidt number of 0.7 is used in the PCs' transport equations.

For computational efficiency, we also carried out the following steps:

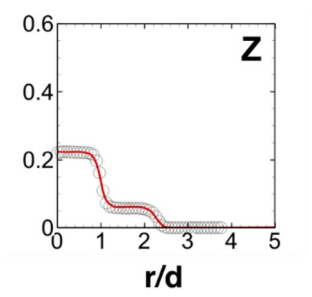
- The unconditional mean chemical source terms for the PCs are pre-computed vs. the
 PCs unconditional means. This process is implemented at every measurement position using the joint PCs PDF at that position and Eq. (3). An artificial neural network
 (ANN) regression is implemented to relate 2 PCs unconditional mean chemical source
 terms to the 2 unconditional means of the PCs.
- Equation (3) also requires calculations of the PCs conditional means as a function of the PCs. This step is implemented after the PMSR calculations and the conversion from thermo-chemical scalars chemical source terms to the PCs source terms (given in Eq. (6)).
- The unconditional means of the thermo-chemical scalars can also pre-computed in terms of the PCs unconditional means at each measurement position. Therefore, once the RANS solution is computed for the unconditional means of the PCs, the 2D fields can readily be converted to the thermo-chemical scalars' unconditional means. Again, we used ANN regression to express this conversion.

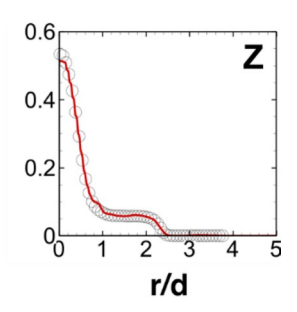
3.3.2 A Posteriori Radial Profiles' Comparisons

In this section, we compare the mean radial profiles obtained from the RANS solution with the experimental radial profiles at different downstream distances. Figure 5 shows comparisons of the mean mixture fraction, Z, at x/d=1 for flames FJ200-5GP-Lr300-59 and FJ200-5GP-Lr75-57. The mixture fraction is based on the Bilger's definition (Bilger et al. 1990). The difference in mixture fraction stratification can be clearly observed here. Flame FJ200-5GP-Lr75-57 (and similarly Flames F200-5GP-Lr75-80 and FJ200-5GP-Lr75-103, not shown here) exhibits greater inhomogeneities and variation along the radial distance.

Figures 6 and 7 compare the mean radial profiles for T and H_2O , H_2 , CO and CO_2 mass fractions and the mixture fraction, Z, at various axial locations, x/d=5, 12, 20 and 30 for Flames FJ200-5GP-Lr75-57 and FJ200-5GP-Lr75-103. Similar comparisons are made for the remaining two flames, F200-5GP-Lr75-80, and FJ200-5GP-Lr300-59 in the Appendix. It may be observed that the results from the closure framework are overall in good

Fig. 5 Comparison of mixture fraction radial profiles at x/d = 1 for the Sydney flames (from left to right) FJ200-5GP-Lr300-59 and FJ200-5GP-Lr75-57







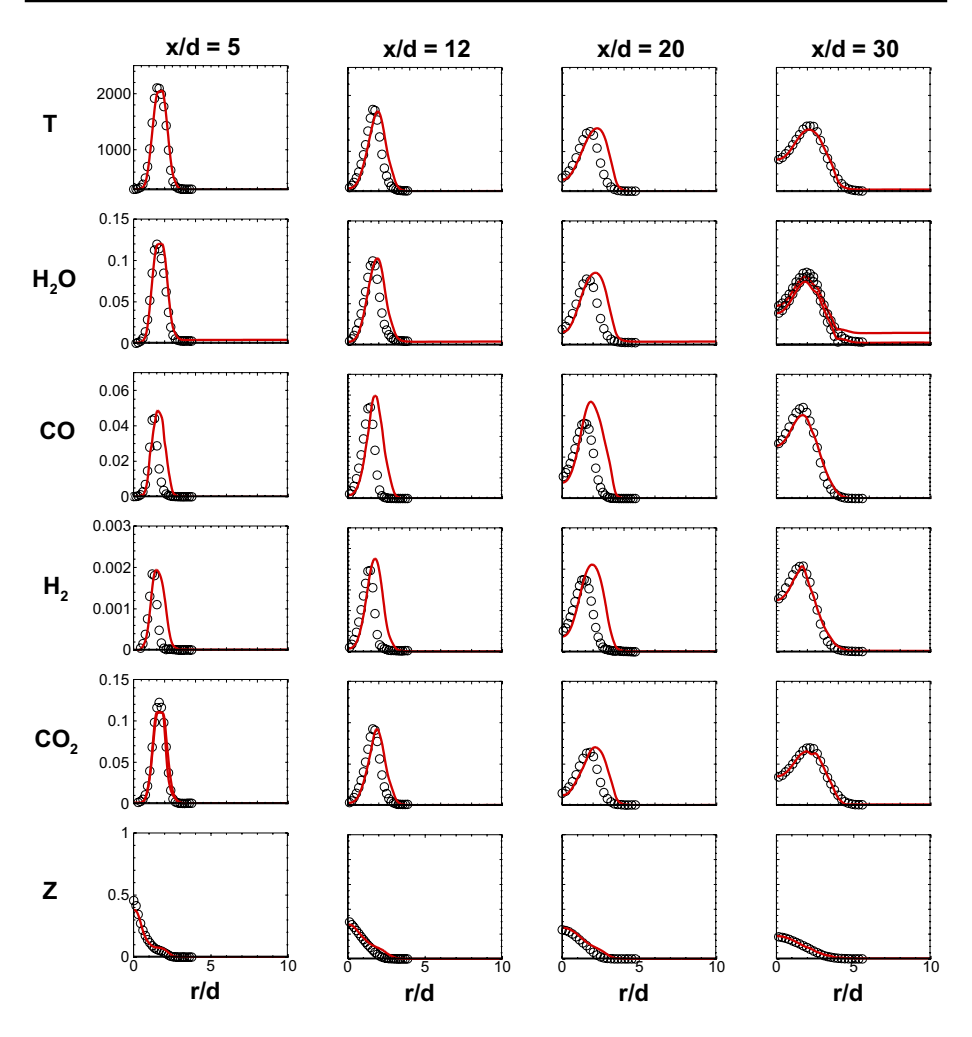


Fig. 6 A posteriori mean radial profile comparison of closure framework (line) and experimental data (symbol) for Sydney flame FJ200-5GP-Lr75-57

agreement with the experimental data. The reignition process is delayed as a function of the Reynolds number. It is important to note that Flame FJ200-5GP-Lr75-103, whose data has not been used in the construction of the framework, also exhibits a reasonably good overall agreement with experimental statistics and shows the trends observed between the flames.

The results based on mean profiles show that the experiment-based framework trained on 4 flames and using 2 PCs to represent the variations in both inlet conditions and to predict process of extinction and reignition are satisfactory. The framework captures reasonably well the effects of variations in inlet mixture and velocity conditions.

Next, we compare the predicted radial profiles of the same measured quantities' RMS values with the experimental statistics corresponding to Figs. 6 and 7. These comparisons are shown in Figs. 8 and 9 for flames FJ200-5GP-Lr75-57 and FJ200-5GP-Lr75-103, respectively. Similar plots for flames FJ200-5GP-Lr75-80 and



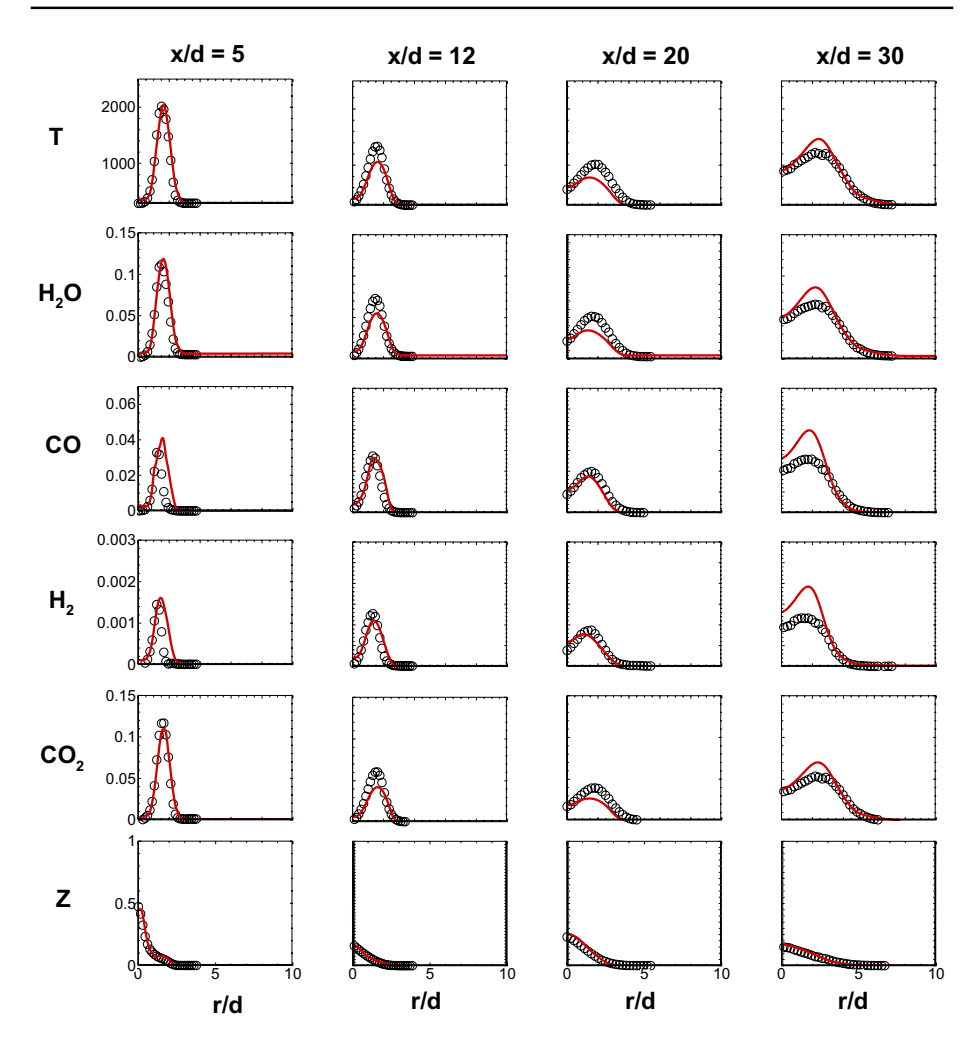


Fig. 7 A posteriori mean radial profile comparison of closure framework (line) and experimental data (symbol) for Sydney flame FJ200-5GP-Lr75-103

FJ200-5GP-Lr300-59 are shown in the Appendix. The most visible trends in the data can be seen further downstream x/d = 20 and 30 where the lower jet Reynolds number flames exhibit higher RMS values in all quantities for the Lr = 75 mm cases. As observed for the mean profiles, the RMS profiles are comparable in magnitudes for all flames.

Based on the above comparisons and despite the presence of some discrepancies between the RMS statistics from the model and the experiment, the overall trends of the RMS profiles across the different flames are reasonably captured both qualitatively and quantitatively. This is the case even for flame FJ200-5GP-Lr75-103, which is not represented in the training for the modeling framework.

At this point, it is useful to compare the present model predictions with those of Perry et al. (2017), Kleinheinz et al. (2017) and Kim and Kim (2017), which adopted different variants of flamelet-based approaches. All these studies, including the present



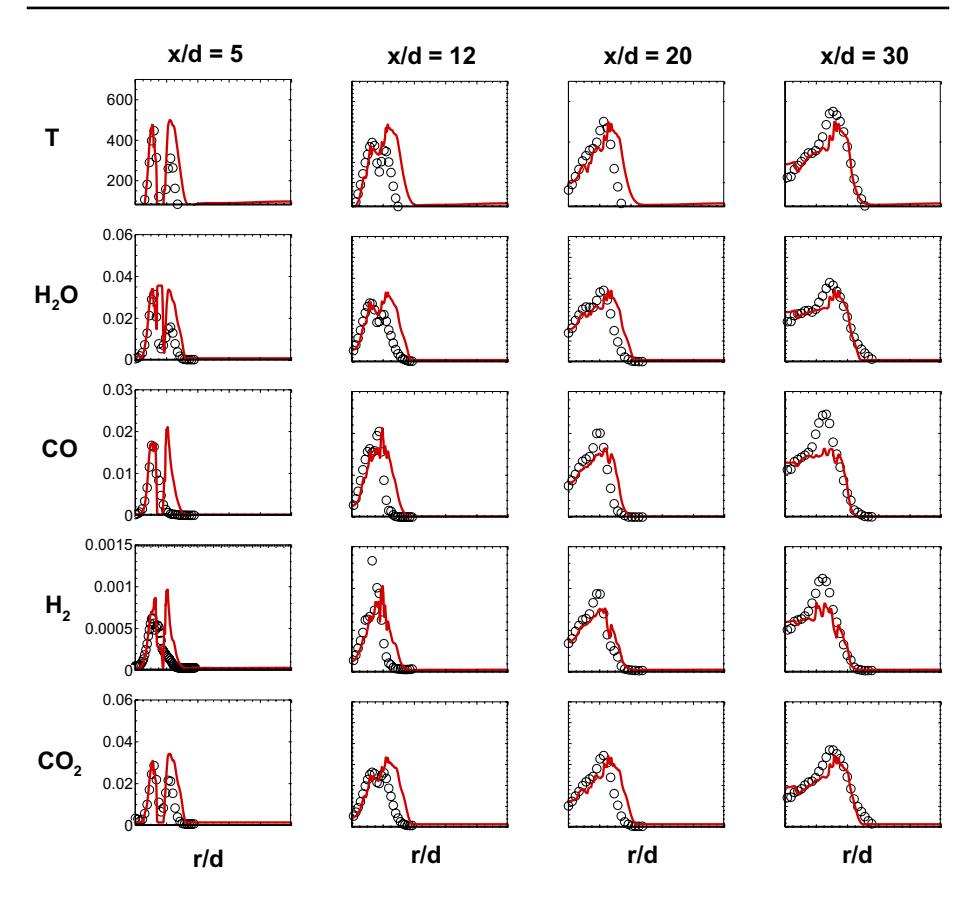


Fig. 8 A posteriori RMS radial profile comparison of closure framework (line) and experimental data (symbol) for Sydney flame FJ200-5GP-Lr75-57

one, have investigated the near-homogeneous flame, FJ200-5GP-Lr300-59, and either one of the inhomogeneous flames, FJ200-5GP-Lr75-57 or FJ200-5GP-Lr-80.

Perry et al. (2017) did not provide radial profiles of unconditional means, although, some results are reported in the Proceedings of the TNF Workshop (Arndt et al. 2018). Mean temperature profiles conditioned on the mixture fractions yielded good comparisons with experimental data while more pronounced deviations are noted for the corresponding H_2 mass fraction statistics. Nonetheless, the choice of a two-mixture fraction outperforms the use of a single mixture fraction.

Kleinheinz et al. (2017) reported radial profiles for unconditional means and RMS for temperature and CO mass fractions for flame FJ200-5GP-Lr75-57. They obtain better predictions at intermediate locations of x/d = 5 and 10, although, both temperature and CO mass fractions are overpredicted at x/d = 30. These over-predictions are consistent with observations made for different models in the TNF Workshop (Arndt et al. 2018). Our present results for the same flame indicate a better agreement at x/d = 30 for both temperature and CO mass fraction.



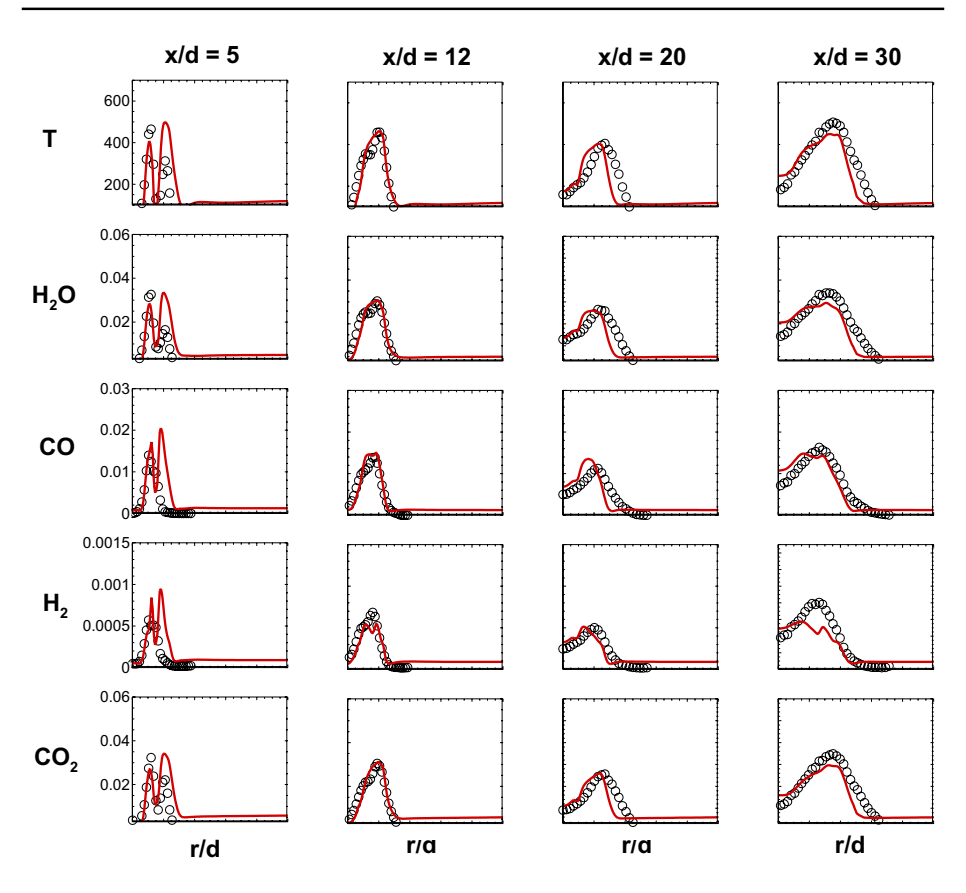


Fig. 9 A posteriori RMS radial profile comparison of closure framework (line) and experimental data (symbol) for Sydney flame FJ200-5GP-Lr75-103

4 Conclusions

In this study, further validation of a novel modeling framework based on multiscalar measurements is carried out using the Sydney flames with inhomogeneous inlets. The mixture, flow and inlet configuration of these flames features different complexities for modeling them. They include the presence of extinction and reignition and multiple combustion modes due to the varying degrees of partial premixing at the inlet.

The modeling framework parameterizes the composition space in terms of PCs instead of the traditional moments, including the mixture fraction and the progress variables. The use of these latter variables is further clouded by ambiguities in defining adequate reference states at the inlet of the Sydney flames. Accordingly, the PCs exhibit different trends based on the degree of partial premixing near the inlet compared to further downstream where non-premixed combustion prevails.

The modeling framework can be implemented a priori to investigate the performance of a number of the framework elements. This is crucial because an a priori validation can be used to determine the adequate number of retained PCs and to assess the adequacy of the data. In the present study, the data is based on 3 flames, which include two different recess



distances for the fuel inlet and different inlet velocities. The a priori validation suggests that 2 PCs are adequate in reproducing measured species and temperature statistics. These 2 PCs can represent the trends in the data associated with different mixture homogeneities at the inlet and the presence of extinction and reignition further downstream.

The a posteriori validation is carried out on the 4 flames (3 flames used to train the model and a fourth flame condition). The comparisons of unconditional mean and RMS computed and measured radial profiles of the measured quantities show a very good agreement. These profiles exhibit similar trends for different inlet velocities and recess lengths. These comparisons are achieved with the some training data from 3 flames.

The present study has demonstrated a unified model that predicts statistics of 4 different flames that exhibit variations in combustion mode and turbulence conditions. These reported results here compared to previous published studies are established using the same pair of PCs constructed from the data of 3 flames. The model's prediction establishes the robustness of this approach. Immediate extensions of the modeling framework must target 2 elements of this framework. The first element is related to the determination of the missing species and the PCs chemical source terms. Data denoising strategies exploiting the inherent correlations of the measured species and temperature will be explored as a complement to the PMSR approach. The second element is related to the construction of the PCs PDF. In a recent study, we have demonstrated a novel approach (Gitushi et al. 2021) that is based on the Deep Operator Network (or DeepONet) (Lu et al. 2021) to construct joint PCs PDFs. The approach has the potential to extend the evaluation of PDFs outside their established range of training.

Finally, it is important to note that the present experiment-based modeling framework can be expanded to incorporate multi-fidelity experimental and computational data. Such expansions can potentially accommodate conditions where measurements are not available or incomplete and where mixture and flow conditions may be different from the measurements. Exploring such expansions has been a proven strategy in combustion modeling. Well-established data-based tabulation approaches, including the steady flamelet (Peters 1984), the flamelet-generated manifolds (FGM) (Oijen and Goey 2000) or the flame prolongation by intrinsic low-dimensional manifolds (FPI) approach (Gicquel et al. 2000) have been enhanced by combining data from distinct reactor simulations (e.g., non-premixed and premixed flames data). However, the addition of stochastic reactor models, such as the partially stirred reactor (PaSR) or PMSRs, can potentially generate statistical distributions in addition to conditional means. Machine learning tools can also serve to enhance the coupling of data originating from different sources or models.

Appendix

In this Appendix, we include additional results of comparisons of mean and RMS profiles of species and temperature corresponding to flames FJ200-5GP-Lr75-80 and FJ200-5GP-Lr300-59. These profiles are shown in Figs. 10 and 11 for the mean profiles of temperature, major species and mixture fraction for flames FJ200-5GP-Lr75-80 and FJ200-5GP-Lr300-59, respectively. Figures 12 and 13 show the corresponding RMS profiles for both flames.

We can equally contrast the prediction of the profiles of flames FJ200-5GP-Lr75-57 (shown in Fig. 6) and FJ200-5GP-Lr300-59 (shown in Fig. 11), which have comparable



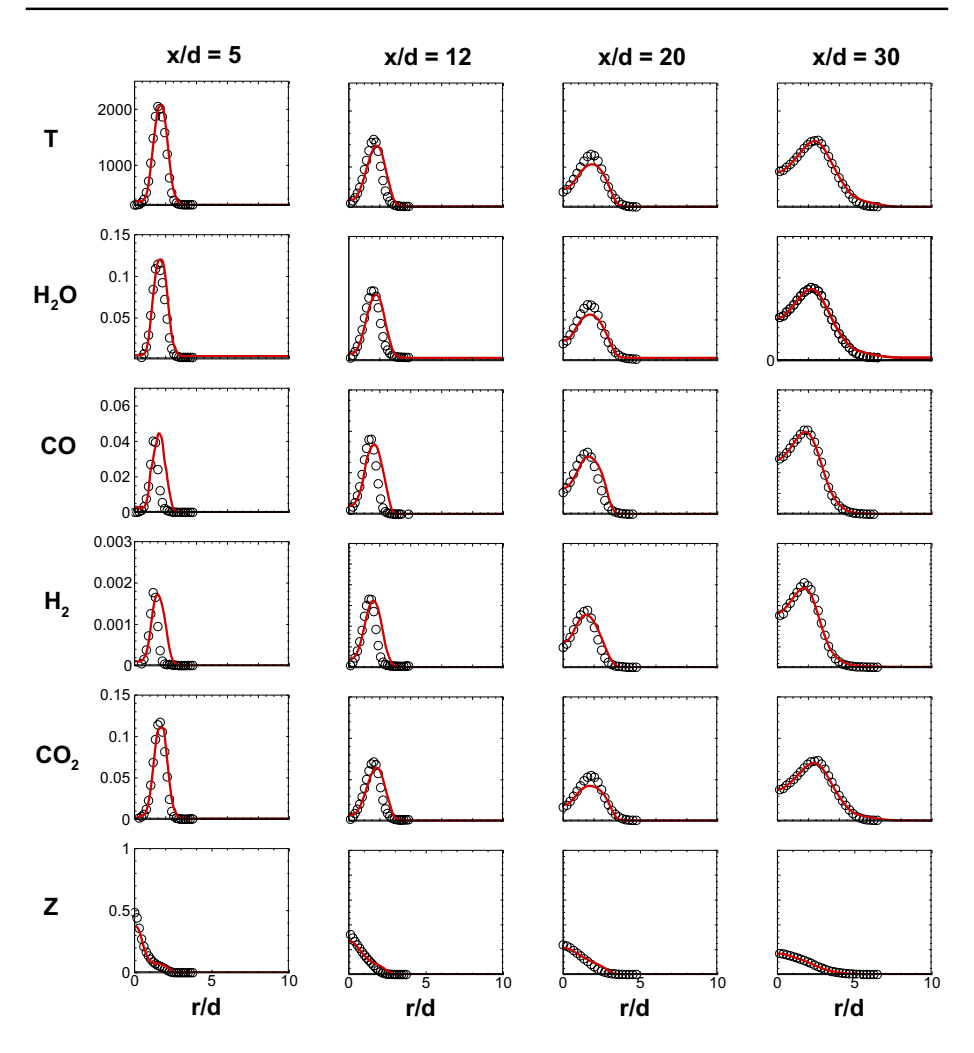


Fig. 10 A posteriori mean radial profile comparison of closure framework (line) and experimental data (symbol) for Sydney flame FJ200-5GP-Lr75-80

inlet velocities and different degrees of inlet inhomogeneities. Although it may not be easily discernable from the plots, there are some variations between the two flames' statistics that are captured by the model. In the near field at x/d = 5 and at x/d = 12, the peak temperature, the products' mass fractions and H_2 mass fraction in FJ200-5GP-Lr75-57 is slightly higher than in FJ200-5GP-Lr300-59. The trends are reversed at x/d = 30 with greater broadening of the mean profiles.

Acknowledgements Dr. Echekki's work is supported by the National Science Foundation under Grant No. 1941430. Dr. Masri is supported by the Australian Research Council.

Funding Dr. Echekki's work is supported by the National Science Foundation under grant no. 1941430. Dr. Masri is supported by the Australian Research Council.



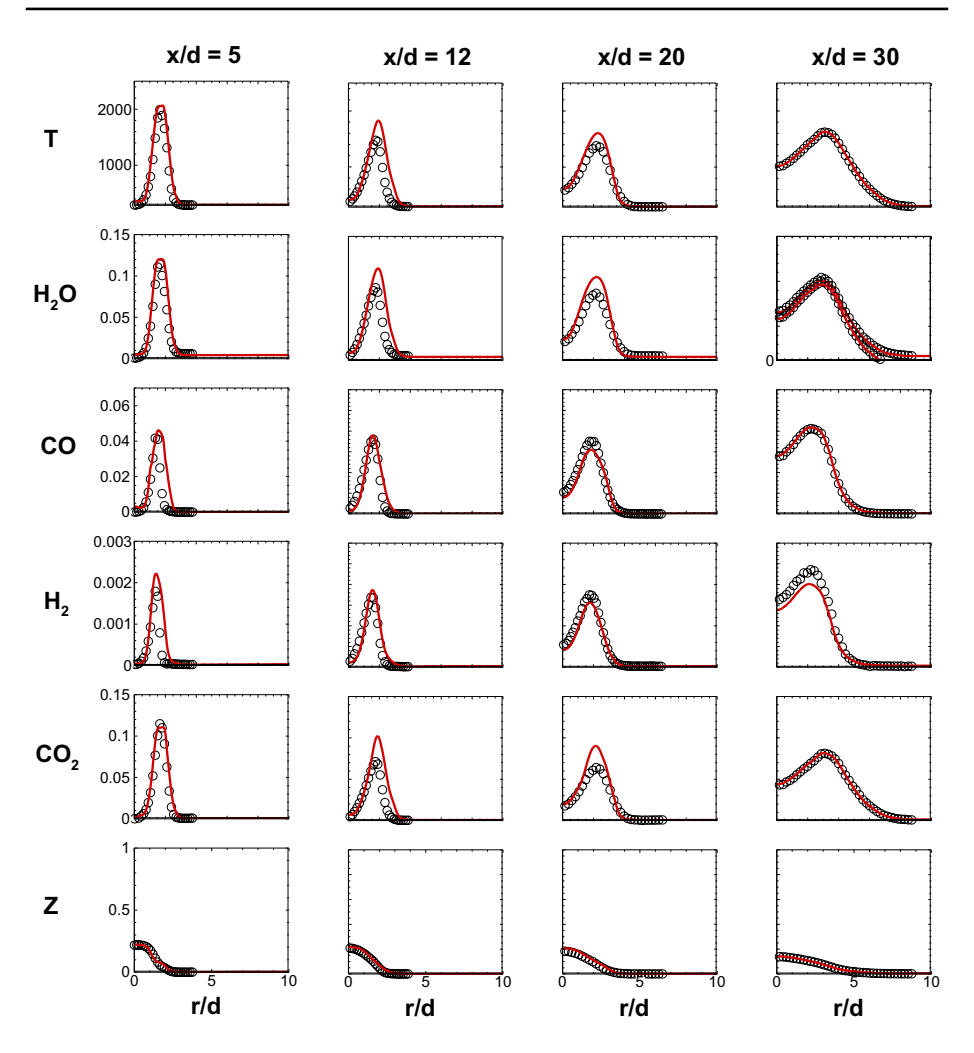


Fig. 11 A posteriori mean radial profile comparison of closure framework (line) and experimental data (symbol) for Sydney flame FJ200-5GP-Lr300-59

Declarations

Conflict of interest We have no competing interests.

Human and Animal Rights This work did not involve any active collection of human data.

References

Arndt, C. Barlow, R.S., Dally, B., Dreizler, A., Fiorina, B., Gordon, R., Hamlington, P., Hawkes, E., Ihme, M., Janicka, J., Kempf, A., Meier, W., Mueller, M., Steinberg, A., Sutton, J., Vervisch, L: Proc. TNF Workshop, July 27–28, 2018, Dublin, Ireland



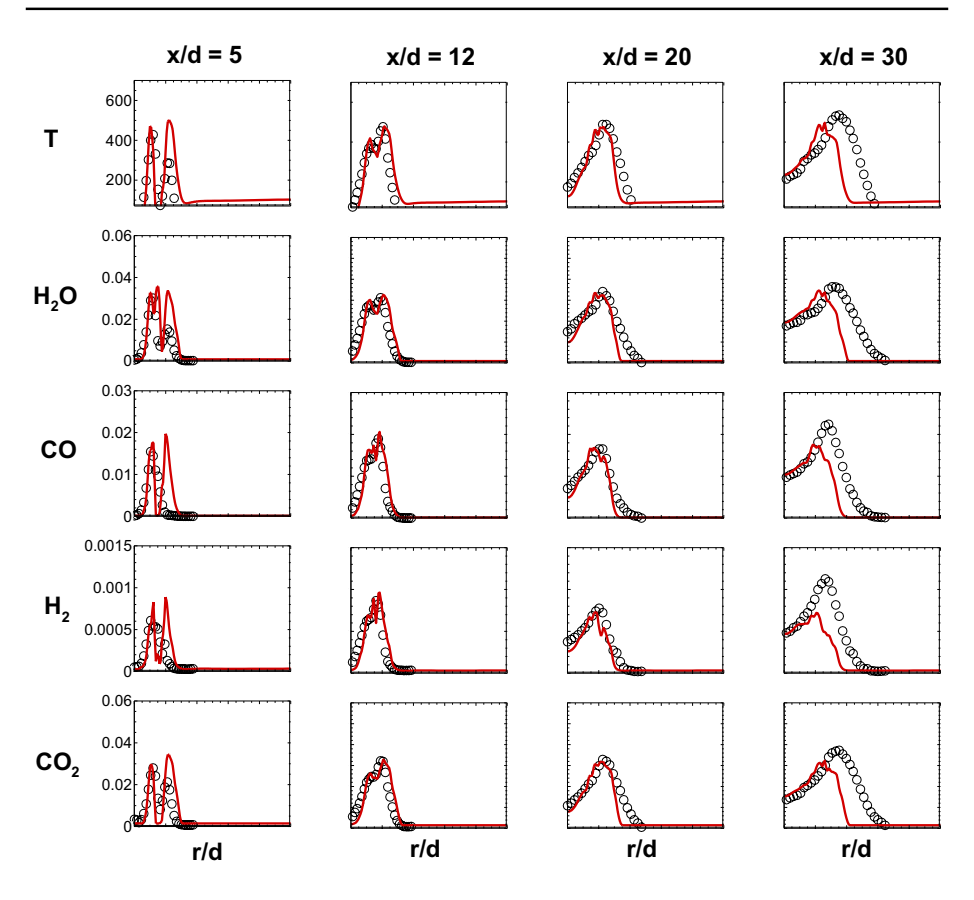


Fig. 12 A posteriori RMS radial profile comparison of closure framework (line) and experimental data (symbol) for Sydney flame FJ200-5GP-Lr75-80

Barlow, R.S., Frank, J.H.: Effects of turbulence on species mass fractions in methane/air jet flames. Proc. Combust. Inst. 27, 1087–1095 (1998)

Barlow, R.S., Meares, S., Magnotti, G., Cutcher, H., Masri, A.R.: Local extinction and near-field structure in piloted turbulent CH4/air jet flames with inhomogeneous inlets. Combust. Flame. 162, 3516–3540 (2015)

Barlow, R.S., Magnotti, G., Cutcher, H.C., Masri, A.R.: On defining progress variable for Raman/Ray-leigh experiments in partially-premixed methane flames. Combust. Flame. **179**, 117–129 (2017)

Bilger, R.W., Starner, S.H., Kee, R.J.: On reduced mechanisms for methane-air combustion in nonpremixed flames. Combust. Flame. 80, 135–149 (1990)

Blasco, J.A., Fueyo, N., Dopazo, C., Ballester, J.: Modelling the temporal evolution of a reduced combustion chemical system with an artificial neural network. Combust. Flame. 113, 38–52 (1998)

Blasco, J.A., Fueyo, N., Larroya, J.C., Dopazo, C., Chen, J.-Y.: A single-step time-integrator of a methane-air chemical system using artificial neural networks. Comp. Chem. Eng. 23, 1127–1133 (1999)

Blasco, J.A., Fueyo, N., Dopazo, C., Chen, J.-Y.: A self-organizing-map approach to chemistry representation in combustion applications. Combust. Theo. Model. 4, 61–76 (2000)

Bowman, A.W., Azzalini, A.: Applied Smoothing Techniques for Data Analysis: The Kernel Approach with S-Plus Illustrations. Oxford University Press, Oxford (1997)

Chatzopoulos, A.K., Rigopoulos, S.: A chemistry tabulation approach via rate-controlled constrained equilibrium (RCCE) and artificial neural networks (ANNs), with application to turbulent non-premixed CH4/H2/N2 flames. Proc. Combust. Inst. 34, 1465–1473 (2013)



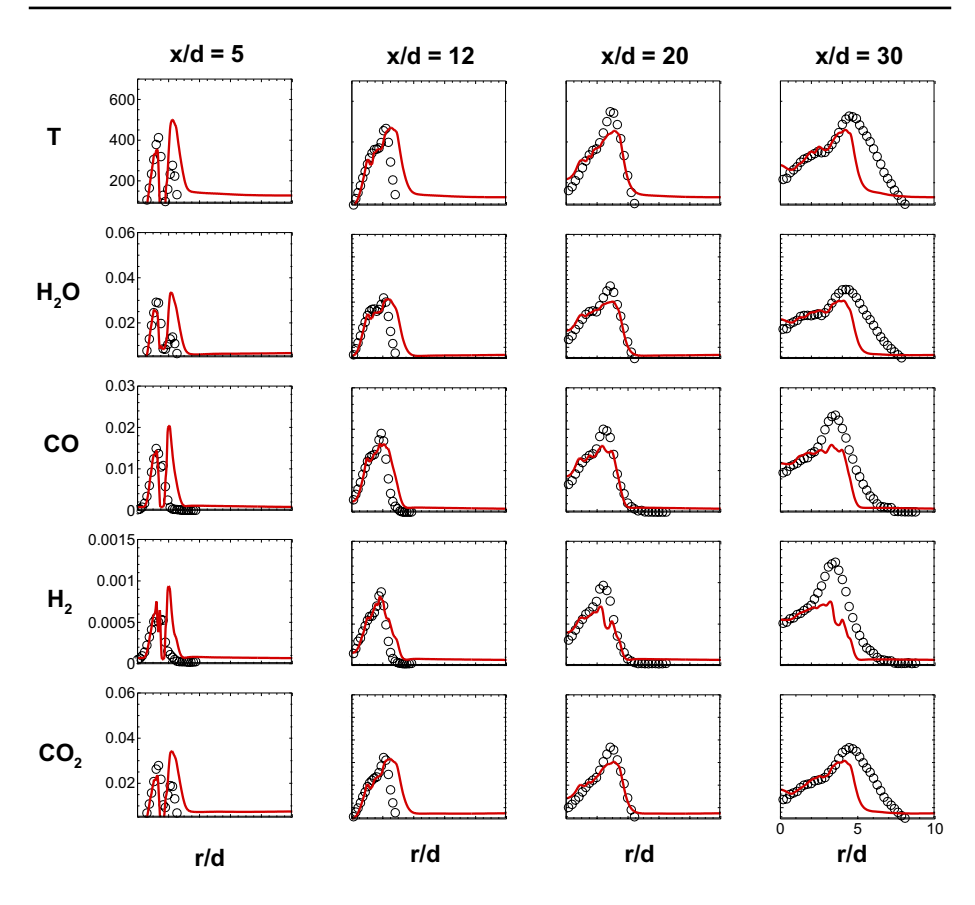


Fig. 13 A posteriori RMS radial profile comparison of closure framework (line) and experimental data (symbol) for Sydney flame FJ200-5GP-Lr300-59

- Chen, J.-Y., Blasco, J.A., Fueyo, N., Dopazo, C.: An economical strategy for storage of chemical kinetics: fitting in situ adaptive tabulation with artificial neural networks. Proc. Combust. Inst. 28, 115–121 (2000)
- Christo, F.C., Masri, A.R., Nebot, E.M., Turanyi, T.: Utilising artificial neural network and repro-modelling in turbulent combustion. Neural Netw. Proc. IEEE Int. Conf. 2, 911–916 (1995)
- Christo, F.C., Masri, A.R., Nebot, E.M., Pope, S.B.: An integrated PDF/neural network approach for simulating turbulent reacting systems. Symp. Combust. 26(1), 43–48 (1996)
- Christo, F.C., Masri, A.R., Nebot, E.M.: Artificial neural network implementation of chemistry with PDF simulation of H₂/CO₂ flames. Combust. Flame. **106**, 406–427 (1996b)
- Coussement, A., Gicquel, O., Parente, A.: Kernel density weighted principal component analysis of combustion processes. Combust. Flame. 159, 2844–2855 (2012)
- Cutcher, H.C., Barlow, R.S., Magnotti, G., Masri, A.R.: Turbulent flames with compositionally inhomogeneous inlets: resolved measurements of scalar dissipation rates. Proc. Combust. Inst. 36, 1737–1745 (2017)
- Echekki, T., Mirgolbabaei, H.: Principal component transport in turbulent combustion: a posteriori analysis. Combust. Flame. 162, 1919–1933 (2015)
- Franke, L.L., Chatzopoulos, A.K., Rigopoulos, S.: Tabulation of combustion chemistry via Artificial Neural Networks (ANNs): methodology and application to LES-PDF simulation of Sydney flame L. Combust. Flame. **185**, 245–260 (2017)
- Galindo, G., Salehi, F., Cleary, M.J., Masri, A.R.: MMC-LES simulations of turbulent piloted flames with varying levels of inlet inhomogeneity. Proc. Combust. Inst. 36, 1759–1766 (2017)



- Galindo-Lopez, S., Salehi, F., Cleary, M.J., Masri, A.R., Neuber, C., Stein, O.T., Kronenburg, A., Varna, A., Hawkes, E.R., Sundaram, B., Klimenko, A.Y., Ge, Y.: A stochastic multiple mapping conditioning computational model in OpenFoam for turbulent combustion. Comput. Fluids. 172, 410–425 (2018)
- Gicquel, O., Darabiha, N., Thevenin, D.: Laminar premixed hydrogen/air counterflow flame simulations using flame prolongation of ILDM with differential diffusion. Proc. Combust. Inst. 28, 1901–1908 (2000)
- Gitushi, K.M., Ranade, R., Echekki, T.: Investigation of deep learning methods for efficient high-fidelity simulations in turbulent combustion, Combust. Flame 236, 111814 (2022)
- Ihme, M., Marsden, A.L., Pitsch, H.: Generation of optimal artificial neural networks using a pattern search algorithm: application to approximation of chemical systems. Neur. Comp. 20, 573–601 (2008)
- Ihme, M., Schmitt, C., Pitsch, H.: Optimal artificial neural networks and tabulation methods for chemistry representation in LES of a bluff-body swirl-stabilized flame. Proc. Combust. Inst. **32**, 1527–1535 (2009)
- Ji, H., Kwon, M., Kim, S., Kim, Y.: Numerical modeling for multiple combustion modes in turbulent partially premixed jet flames. J. Mech. Sci. Tech. 32, 5511–5519 (2018)
- Kim, N., Kim, Y.: Multi-environment probability density function approach for turbulent partially-premixed methane/air flame with inhomogeneous inlets. Combust. Flame. **182**, 190–205 (2017)
- Kleinheinz, K., Kubis, T., Trisjono, P., Bode, M., Pitsch, H.: Computational study of flame characteristics of a turbulent piloted jet burner with inhomogeneous inlets. Proc. Combust. Inst. 36, 1747–1757 (2017)
- Kohonen, T.: Self-organized formation of topologically correct featured maps. Bio. Cyber. 43, 59-69 (1982)
- Lu, L., Jin, P., Pang, G., Zhang, Z., Karniadakis, G.E.: Learning nonlinear operators via DeepONet based on the universal approximation theorem of operators. Nat. Mach. Intell. 3, 218–229 (2021)
- Maio, G., Cailler, M., Darabiha, N., Fiorina, B.: Capturing multi-regime combustion in turbulent flames with a virtual chemistry approach. Proc. Combust. Inst. 38, 2559–2569 (2021)
- Meares, S., Masri, A.R.: A modified piloted burner for stabilizing turbulent flames of inhomogeneous mixtures. Combust. Flame. 161, 484–495 (2014)
- Meares, S., Prasad, V.N., Magnotti, G., Barlow, R.S., Masri, A.R.: Stabilization of piloted turbulent flames with inhomogeneous inlets. Proc. Combust. Inst. 35, 1477–1484 (2015)
- Mirgolbabaei, H., Echekki, T.: A novel principal component analysis-based acceleration scheme for LES–ODT: An a priori study. Combust. Flame. **161**, 898–908 (2013)
- Mirgolbabaei, H., Echekki, T.: Nonlinear reduction of combustion composition space with kernel principal component analysis. Combust. Flame. **161**, 118–126 (2014)
- Mirgolbabaei, H., Echekki, T.: The reconstruction of thermo-chemical scalars in combustion from a reduced set of their principal components. Combust. Flame. **162**, 1650–1652 (2015)
- Mirgolbabaei, H., Echekki, T., Smaoui, N.: A nonlinear principal component analysis approach for turbulent combustion composition space. Int. J. Hydrogen Energy. 39, 4622–4633 (2014)
- Owoyele, O., Echekki, T.: Toward computationally efficient combustion DNS with complex fuels via principal component transport. Combust. Theo. Model. 21, 770–798 (2017)
- Owoyele, O., Kundu, P., Ameen, M.M., Echekki, T., Som, S.: Application of deep artificial neural networks to multi-dimensional flamelet libraries and spray flames. Int. J. Eng. Res. 21, 151–168 (2019)
- Parente, A., Sutherland, J.C., Dally, B.B., Tognotti, G., Smith, P.J.: Investigation of the MILD combustion regime via principal component analysis. Proc. Combust. Inst. 33, 3333–3341 (2011)
- Perry, B.A., Mueller, M.E.: Effect of multiscalar subfilter PDF models in LES of turbulent flames with inhomogeneous inlets. Proc. Combust. Inst. 37, 2287–2295 (2019)
- Perry, B.A., Mueller, M.E., Masri, A.R.: A two mixture fraction flamelet model for large eddy simulation of turbulent flames with inhomogeneous inlets. Proc. Combust. Inst. 36, 1767–1775 (2017)
- Peters, N.: Laminar diffusion flamelet models in non-premixed turbulent combustion. Prog. Energy Combust. Sci. 10, 319–329 (1984)
- Pope, S.B.: Computationally efficient implementation of combustion chemistry using in-situ tabulation. Combust. Theo. Model. 1, 41–63 (1997)
- Ranade, R., Echekki, T.: A framework for data-based turbulent combustion closure: a priori validation. Combust. Flame. 206, 490–505 (2019a)
- Ranade, R., Echekki, T.: A framework for data-based turbulent combustion closure: a posteriori validation. Combust. Flame. **210**, 279–291 (2019b)
- Ranade, R., Alqahtani, S., Farooq, A., Echekki, T.: An ANN based hybrid chemistry framework for complex fuels. Fuel **241**, 625–636 (2019a)
- Ranade, R., Alqahtani, S., Farooq, A., Echekki, T.: An extended hybrid chemistry framework for complex hydrocarbon fuels. Fuel **251**, 276–284 (2019b)
- Ranade, R., Li, G., Li, S., Echekki, T.: An efficient machine-learning approach for PDF tabulation in turbulent combustion closure. Combust. Sci. & Tech. 193, 1258–1277 (2021)



- Sen, B.A., Menon, S.: Linear eddy mixing based tabulation and artificial neural networks for large eddy simulations of turbulent flames. Combust. Flame. 157, 62–74 (2010)
- Sen, B.A., Hawkes, E.R., Menon, S.: Large eddy simulation of extinction and reignition with artificial neural networks based chemical kinetics. Combust. Flame. **157**, 566–578 (2010)
- Shih, T.H., Liou, W.W., Shabbir, A., Yang, Z., Zhu, J.: A new k-ε viscosity model for high Reynolds number turbulent flows. Comput. Fluids **24**, 227–238 (1995)
- Sutherland, J.C., Parente, A.: Combustion modeling using principal component analysis. Proc. Combust. Inst. 32, 1563–1570 (2009)
- van Oijen, J.A., de Goey, L.P.H.: Modeling of premixed laminar flames using flamelet-generated manifolds. Combust. Sci. Tech. 161, 113–137 (2000)
- Wu, H., Ihme, M.: Compliance of combustion models for turbulent reacting flow simulations. Fuel 186, 853–863 (2016)
- Yang, B., Pope, S.B.: An investigation of the accuracy of manifold methods and splitting schemes in the computational implementation of combustion chemistry. Combust. Flame. 112, 16–32 (1998)

Publisher's Note Springer Nature remains neutral with regard to jurisdictional claims in published maps and institutional affiliations.

